frontiers | Frontiers in Soft Matter

TYPE Original Research
PUBLISHED 11 October 2022
DOI 10.3389/frsfm.2022.1011618

OPEN ACCESS

EDITED BY
Hiroshi Yokoyama,
Kent State University, United States

REVIEWED BY
Alejandro D. Rey,
McGill University, Canada
Miha Ravnik,
University of Ljubljana, Slovenia

*CORRESPONDENCE
Jun-ichi Fukuda,
fukuda.jun-ichi@phys.kyushu-u.ac.jp

SPECIALTY SECTION
This article was submitted to Liquid Crystals,
a section of the journal
Frontiers in Soft Matter

RECEIVED 04 August 2022
ACCEPTED 05 September 2022
PUBLISHED 11 October 2022

CITATION
Fukuda J-i (2022), Simulation of a cholesteric blue phase cell with large but finite thickness.
Front. Soft. Matter 2:1011618.
doi: 10.3389/frsfm.2022.1011618

Simulation of a cholesteric blue phase cell with large but finite thickness

Jun-ichi Fukuda*

Department of Physics, Kyushu University, Fukuoka, Japan

We investigate the structure of a cholesteric blue phase (BP) liquid crystal cell of finite thickness under an electric field normal to the planar surfaces confining the liquid crystal. We carry out large scale simulations to consider cases in which the thickness of the BP liquid crystal is approximately 40 times the BP lattice constant (typical thickness in experiments), larger than that of previous simulation studies. Our calculations clearly demonstrate that the number of periodic structures along the thickness direction (thickness divided by the lattice constant) is discretized by the presence of confining surfaces. The stability of the so-called BP X structure over the BP I under the electric field, as well as the electrostriction, is confirmed. The metastability of the BP X structure after the cessation of the electric field, demonstrated in a recent experiment [Nat. Mater. **19**, 94 (2020)] is also shown. We also perform calculations for the reflection spectra of the BP structures, and clearly observe the shift of the reflection peak due to electrostriction. Our study demonstrates the role of finite thickness on the behavior of a BP cell.

KEYWORDS

cholesteric blue phase, liquid crystal cell, electric field, electrostriction, reflection spectrum

Introduction

Cholesteric blue phases (BPs) are complex three-dimensional ordered structures exhibited by highly chiral liquid crystals (Wright and Mermin 1989; Bahr and Kitzerow 2001). They comprise an intricate network of so-called double-twist cylinders and topological line defects of orientational order (disclination lines). In a double-twist cylinder, the orientational order is twisted along all directions perpendicular to the cylinder axis. Two thermodynamically stable blue phases are known to exhibit cubic symmetry: BP I with body-centered-cubic ordering with space group O_8 ($I4_132$), and BP II with simple cubic ordering with space group O_2 ($P4_232$) (A third stable blue phase, BP III, which is believed to be amorphous (Henrich et al., 2011; Gandhi and Chien 2017), is not the target of the present study). Cholesteric blue phases have been attracting interest from the viewpoint of basic science as an intriguing example of frustration-induced order (The inability of energetically favorable double-twist ordering to fill the whole space leads to the formation of disclination lines), and extensive studies have been carried out towards

application for fast-switching displays (Kikuchi et al., 2002, 2007; Rahman et al., 2015; Tan et al., 2017).

The response of cholesteric blue phases to an applied electric field has been drawing considerable attention because it provides an interesting problem on structural transformation in soft materials, and its understanding is crucial for their potential applications. The electric field gives rise to intriguing behavior involving the change in the symmetry and the variation of lattice constants (electrostriction) (Kitzerow 1991). Hexagonal (Pieranski et al., 1985; Hornreich and Shtrikman 1989) and tetragonal (Cladis et al., 1986; Pieranski and Cladis 1987) blue phases have been identified that are thermodynamically stable only under an electric field. The latter, often referred to as BP X, has been shown to possess the space group symmetry $I4_122$. Electrostriction of BPs and the resulting shift of reflection peak have been also attracting interest because of the potential of BPs as a tunable photonic material (Heppke. et al., 1989b; Yoshida et al., 2013; Chen et al., 2015; Guo et al., 2020).

Here we carry out a simulation study on how an applied electric field affect the structural and optical properties of a BP cell whose thickness is comparable with that of a real experimental cell (~ 10 μm). Our study is motivated by a recent experimental study (Guo et al., 2020) that demonstrated that BP X structures with their lattice constant along the cell normal being larger than that of BP I can be stable even after the cessation of the electric field (to be precise, they are metastable but their lifetime is long enough for applications). (Meta)stable BP X has been achieved by carefully applying an electric field repetitively with time intervals so that the BP can effectively dissipate heat during the interval. The lattice constant of the observed metastable BP X along the cell normal is not unique and depends on the history of the applied field. Purely bulk BPs are not likely to exhibit multiple lattice constants, and therefore the finite thickness and the presence of confining surfaces seem to play some role.

There have been a number of simulation studies focusing on the behavior of BPs under an electric field (Alexander and Marenduzzo 2008; Alexander and Yeomans 2009; Fukuda et al., 2009; Fukuda and Žumer 2013; Henrich et al., 2010; Tiribocchi et al., 2011a; 2011b). However, most of them deal with purely bulk systems with periodic boundary conditions, or, even when a cell of finite thickness is considered, the cell thickness is much smaller than that of typical experimental systems. In the present work, the cell thickness is taken to be $30\sqrt{2}$ times the lattice constant of bulk BP I, which corresponds to ~ 10 μm, close to typical experimental values. Note that in a previous large scale simulation of BPs (although the electric field is not considered) (Li et al., 2017; Martínez-González et al., 2017), the cell thickness is 2.1 μm, 14 times the lattice constant of BP (Note also that the lateral dimension of their numerical BP cell is a few times larger than ours). Although there are a number of possibilities for the lattice orientation of BPs, because of the high numerical costs, we restrict our attention to two cases typically observed experimentally (Yoshida et al., 2013; Chen et al., 2015; Guo et al., 2020): BP I with its (110) plane parallel to the confining surfaces, and BP X with its 4_1 screw axis along the cell normal.

This paper is organized as follows: In *Calculation of BP structures* and *Calculation of reflection spectra*, respectively, we describe how we calculate the structures of BPs and their reflection spectra. The results of the calculation of the structures are shown in *Structures of cholesteric blue phase in a cell* and *Reflection spectra* presents the reflection spectra. *Discussion* gives a concluding discussion.

Model

Calculation of BP structures

For the calculation of the structures of our cholesteric blue phase cell, we make use of the Landau-de Gennes continuum theory in which the orientational order of the liquid crystal is represented by a second-rank symmetric and traceless tensor $\chi_{\alpha\beta}$. Details of the theory and the numerical calculation are presented in our previous papers (Fukuda et al., 2009; Fukuda and Žumer 2010a; 2010b; Fukuda and Žumer 2011a; 2011b; Nych et al., 2017; Fukuda et al., 2018; Fukuda and Žumer 2020; Fukuda 2022; Fukuda et al., 2022), and here we present their essence.

The geometry of the liquid crystal cell, shown in Figure 1, is such that it is confined by two planar surfaces that are parallel to the xy plane and located at $z = 0$ and $z = L$ (The cell thickness is hence L. As mentioned below, length is appropriately rescaled). The free energy of the liquid crystal is given as a functional of the order parameter $\chi_{\alpha\beta}(\boldsymbol{r})$, where $\boldsymbol{r}$ represents the position. We introduce the rescaling of the free energy itself, order parameter, length and the material parameters as described in detail in Supplementary Appendix S1. The total free energy is the sum of the bulk part and the surface anchoring part, and the former is written as

$$F_{\text{bulk}} = \int dx\, dy \int_0^L dz\, [\varphi_{\text{local}}(\chi) + \varphi_{\text{elastic}}(\chi, \nabla) + \varphi_E(\chi)], \quad (1)$$

where

$$\varphi_{\text{local}}(\chi) = \tau\, \text{Tr}\chi^2 - \sqrt{6}\, \text{Tr}\chi^3 + (\text{Tr}\chi^2)^2, \quad (2)$$

is the local free energy given as a Landau expansion in terms of $\chi_{\alpha\beta}$, and τ is the rescaled temperature. Tr means the trace of a tensor. The elastic energy taking care of the inhomogeneity of $\chi_{\alpha\beta}$ is written as

$$\varphi_{\text{elastic}}(\chi, \nabla) = \kappa^2 \left\{ \left[(\nabla \times \chi)_{\alpha\beta} + \sigma\chi_{\alpha\beta} \right]^2 + \eta \left[(\nabla \cdot \chi)_\alpha \right]^2 \right\}, \quad (3)$$

where κ is the rescaled elastic constant and can be regarded also as the strength of chirality inversely proportional to the cholesteric pitch p (See Supplementary Appendix S1). The

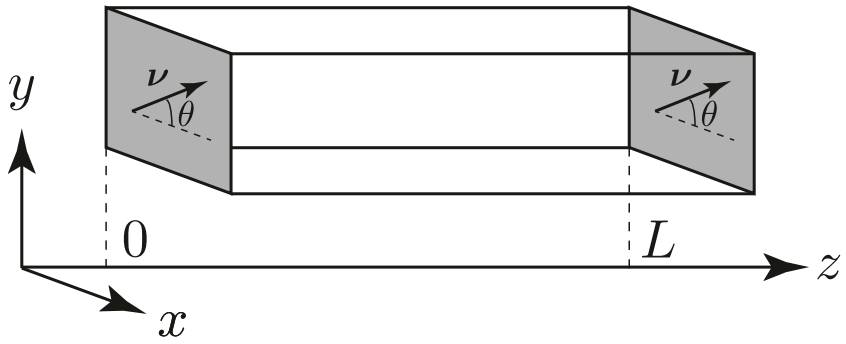

FIGURE 1
Geometry of the system for numerical calculation. The gray planes at $z = 0$ and L are the cell surfaces imposing unidirectional planar anchoring with its easy axis being $\boldsymbol{\nu}$. The angle *theta* specifies the direction of $\boldsymbol{\nu}$ with respect to the x axis. Other white planes impose periodic boundary conditions.

parameter η represents the anisotropy of elasticity. In the present study η is set to one corresponding to the so-called one-constant approximation setting the splay, twist and bend Frank elastic constants to be equal. We have adopted this approximation just for simplicity, and in usual nematic liquid crystal made of rodlike molecules, twist elastic constant is smaller than the other two, and smaller twist elastic constant is realized by taking $\eta > 1$ (Wright and Mermin 1989; Fukuda 2022). Here and in the following, summations over repeated Greek indices are implied (Hence, in Eq. 3, the summation symbols $\sum_{\alpha=x,y,z}$ and $\sum_{\beta=x,y,z}$ are omitted). Note that the length has been rescaled so that the cholesteric pitch is equal to 4π (See Appendix). Therefore the cholesteric pitch does not appear explicitly in Eq. 3. The sign of the chirality is determined by that of σ ($|\sigma| = 1$) and we here choose $\sigma = +1$, which yields right-handed helical order in the terminology of de Gennes and Prost 1995. The electrostatic energy is given by

$$\varphi_E(\chi) = -\tilde{\epsilon}\hat{e}_\alpha\hat{e}_\beta\chi_{\alpha\beta}, \tag{4}$$

where the electric field is assumed to be uniform and fixed, and the unit vector $\hat{\boldsymbol{e}}$ is along the field direction. The parameter $\tilde{\epsilon}$ characterizes the effect of the field, and is proportional to the dielectric anisotropy (including its sign), and the square of the field strength. In the present study we consider the case of positive dielectric anisotropy, and for simplicity the electric field is assumed to be uniform along the cell normal (z direction).

The surface anchoring energy is expressed as

$$F_{\rm surf} = \int dx\,dy\{\varphi_{s0}(\chi) + \varphi_{sL}(\chi)\}, \tag{5}$$

where $\varphi_{s0}(\chi)$ and $\varphi_{sL}(\chi)$ are the free energy density at $z = 0$ and $z = L$, respectively. As in our previous study (Fukuda and Žumer 2020), both $\varphi_{s0}(\chi)$ and $\varphi_{sL}(\chi)$ are given by the sum of the planar-degenerate part $\varphi_{\rm pd}$ and the unidirectional planar part $\varphi_{\rm pd}$ that are expressed as

$$\varphi_{\rm pd}(\chi) = \frac{1}{2}w_1{\rm Tr}(\tilde{\chi} - \tilde{\chi}^{\perp})^2 + \frac{1}{2}w_2({\rm Tr}\tilde{\chi}^2 - \chi_s^2)^2, \tag{6}$$

$$\varphi_{\rm ud}(\chi) = \frac{1}{2}w_{\rm ud}{\rm Tr}(\chi - \chi_0)^2. \tag{7}$$

Eq. 6, originally proposed in Fournier and Galatola 2005, has been extensively used for modeling surfaces with planar-degenerate anchoring with no preferred in-plane orientation. In Eq. 6, χ_s defines the degree of orientational order at the surface, $\tilde{\chi}_{\alpha\beta} \equiv \chi_{\alpha\beta} + (1/3)\chi_s\delta_{\alpha\beta}$ and $\tilde{\chi}^{\perp}_{\alpha\beta} \equiv P_{\alpha\mu}\tilde{\chi}_{\mu\nu}P_{\nu\beta}$ with $P_{\alpha\beta} = \delta_{\alpha\beta} - \delta_{\alpha z}\delta_{\beta z}$ being the projection operator onto the surface (parallel to the xy plane in the present case). In Eq. 7, χ_0 is the value of the tensor order parameter that minimizes $\varphi_{\rm ud}$, and we set

$$\chi_{0\alpha\beta} = \chi_s\left(\nu_\alpha\nu_\beta - (1/3)\right)\delta_{\alpha\beta}. \tag{8}$$

Here $\boldsymbol{\nu}$ is the direction of the orientational order imposed by the unidirectional planar anchoring (hereafter referred to as the easy axis), and taken to be parallel to the xy plane. Therefore $\boldsymbol{\nu}$ can be written as $\boldsymbol{\nu} = (\cos\theta, \sin\theta, 0)$, with θ being the azimuthal angle of the easy axis (Figure 1). The parameters w_1, w_2 and $w_{\rm ud}$ are rescaled anchoring strengths. In our system, θ is taken to be the same for both surfaces. In Fukuda and Žumer 2020, we discussed how the variation of θ affects the free energy of BP I with its (110) planes parallel to the confining surfaces. We showed that the free energy is minimized at $\theta = 38.5^\circ$. Similar calculation for BP X shows that $\theta = 38.5^\circ$ minimizes the free energy of BP X as well, although we believe that this is a coincidence without a profound meaning (Note that the precision of θ is 0.1°). From these observations, we set $\theta = 38.5^\circ$ for the present calculations.

For the convenience of the discussions that follow, we define the free energy per (rescaled) unit area:

TABLE 1 Summary of parameters used for all the simulations. See Supplementary Appendix S1 for the correspondence between the parameters and the corresponding parameters before rescaling.

Symbol	Value	Corresponding value before rescaling
κ	0.4	pitch $p \simeq 280$ nm
τ	−0.1	(BP I is thermodynamically stable)
η	1	(One-constant approximation)
w_1, w_2	0.1	anchoring strength $\simeq 7 \times 10^{-5}$ Jm^{-2}
w_{ud}	0.025	anchoring strength $\simeq 1.7 \times 10^{-5}$ Jm^{-2}
χ_s	0.994	(minimizes φ^{local} at $\tau = -0.1$)
L	536.673	$\simeq 12\ \mu$m ($30\sqrt{2}$ times the lattice constant of bulk BP I)
$\tilde{\epsilon}$	0.02 0.03	electric field $\simeq$ 3.2V/μm 3.9V/μm

$$\mathcal{F} = \frac{F_{\text{bulk}} + F_{\text{surf}}}{\int dx\, dy}, \tag{9}$$

where F_{bulk} and F_{surf} are defined in Eqs. 1, 5, respectively.

In Table 1 we summarize the parameters used for all the simulations. See Supplementary Appendix S1 for more detail on how Table 1 is derived. As noted above, we consider the case of positive dielectric anisotropy ($\tilde{\epsilon} > 0$), and set $\tilde{\epsilon}$ to 0, 0.02 and 0.03. Separate calculations for a bulk system shows that the phase transition between BP I and BP X occurs at $\tilde{\epsilon} \simeq 0.02$, corresponding to $E \simeq 3.2$ V/μm (Table 1), close to typical experimental transition field strength ($\simeq 3.0$ V/μm in Guo et al., 2020). We also note that for our choice of $\kappa = 0.4$ (corresponding to $p \simeq 280$ nm), the free energy before rescaling per μm^2 is

$$\simeq \mathcal{F} \times 6.8 \times 10^4 k_B T, \tag{10}$$

where $\mathcal{F}$ is defined in Eq. 9, k_B is the Boltzmann constant, and $k_B T \simeq 4.1 \times 10^{-21}$ J for room temperature (See Supplementary Appendix S1).

In the xy plane, periodic boundary conditions are imposed, and the system is discretized by $N_x \times N_y$ rectangular grid points with spacings Δ_x and Δ_y. We have chosen $N_x = 45$ and $N_y = 32$. In the z direction normal to the confining surfaces, $N_z + 1$ grid points with equal spacings Δ_z and $N_z = 1350$ are allocated (Hence the cell thickness is $L = N_z \Delta_z$). The minimization of the free energy is achieved by a simple relaxation equation:

$$\frac{\partial}{\partial t}\chi_{\alpha\beta}(\boldsymbol{r}) = -\frac{\delta(F_{\text{bulk}} + F_{\text{surf}})}{\delta \chi_{\alpha\beta}(\boldsymbol{r})} + \lambda(\boldsymbol{r})\delta_{\alpha\beta}, \tag{11}$$

where $\lambda(\boldsymbol{r})$ is the Lagrange multiplier ensuring the tracelessness of $\chi_{\alpha\beta}(\boldsymbol{r})$, and the time t is rescaled so that the kinetic coefficient does not appear explicitly in Eq. 11. The technical details of the minimization procedures are described in detail in Fukuda and Žumer 2020. We just note here that not only the order parameter $\chi_{\alpha\beta}$ but also Δ_x and Δ_y are optimized in the minimization procedures.

Initial conditions necessary for the minimization procedure of the free energy are prepared as follows. In a smaller system with periodic boundary conditions in the x, y and z direction, we prepare a profile of BP I with its (110) plane parallel to the xy plane, and a profile of BP X. The initial condition is the repetition of one of these profiles along the z direction. We prepare different initial conditions containing different numbers of BP lattices in the z direction of the BP cell by changing the lattice constant of the BP lattice in the z direction.

Calculation of reflection spectra

For reflection spectra, we solve the Maxwell equations for electromagnetic wave of light as described in our previous studies (Fukuda et al., 2016; Nych et al., 2017; Fukuda and Žumer 2018; Cho et al., 2021). For a non-magnetic medium with no free charge or electric current, the magnetic field is safely eliminated and the Maxwell equation for the electric field $\boldsymbol{E}$ oscillating with a single frequency ω as $\propto \exp(-i\omega t)$ reads (Landau et al., 1984)

$$\nabla\times\nabla\boldsymbol{E} - \left(\frac{\omega}{c}\right)^2 \overleftrightarrow{\epsilon}\boldsymbol{E} = 0. \tag{12}$$

Here $\overleftrightarrow{\epsilon}$ is the dielectric tensor and c is the speed of light in vacuum.

As noted in *Calculation of reflection spectra*, the liquid crystal fills the region $0 \le z \le L$. The media outside the liquid crystal ($z < 0$, $z > L$) are an isotropic and homogeneous materials whose refractive index is set to $n_{\text{outside}} = 1.5$ (or the dielectric constant $\epsilon_{\text{outside}} = 2.25$). The dielectric tensor of the liquid crystal is assumed to be a linear function of the order parameter, that is, $\epsilon_{\alpha\beta} = \epsilon_{\text{iso}}\delta_{\alpha\beta} + \epsilon_a \chi_{\alpha\beta}$, where $\epsilon_{\text{iso}} = 2.571$ and $\epsilon_a = 0.825$ as in the previous studies (Nych et al., 2017), and $\delta_{\alpha\beta}$ is the Kronecker delta. The choice of ϵ_{iso} and ϵ_a is such that the average refractive index of the liquid crystal is $n_{\text{LC}} = 1.6$, close to typical experimental values.

We consider the response of the liquid crystal to monochromatic light incident from $z = -\infty$, whose electric field is given by $\boldsymbol{E} = \boldsymbol{E}_i \exp(i\boldsymbol{k}_i \cdot \boldsymbol{r})$. As noted in *Calculation of reflection spectra* we assume the periodicity of $\chi_{\alpha\beta}$ in the xy direction, and then according to the Bloch theorem the electric field $\boldsymbol{E}$ is formally expanded as

$$\boldsymbol{E}(\boldsymbol{r}_\perp, z) = \begin{cases} \boldsymbol{E}_i \exp(i\boldsymbol{k}_i \cdot \boldsymbol{r}) + \sum_{m,n} \boldsymbol{E}_r^{(m,n)} \exp\left[i\left(\boldsymbol{k}_\perp^{(m,n)} \cdot \boldsymbol{r}_\perp + k_{rz}^{(m,n)} z\right)\right] & (z < 0), \\ \sum_{m,n} \boldsymbol{E}_{LC}^{(m,n)}(z) \exp\left(i\boldsymbol{k}_\perp^{(m,n)} \cdot \boldsymbol{r}_\perp\right) & (0 < z < L), \\ \sum_{m,n} \boldsymbol{E}_t^{(m,n)} \exp\left[i\left(\boldsymbol{k}_\perp^{(m,n)} \cdot \boldsymbol{r}_\perp + k_{tz}^{(m,n)}(z - L)\right)\right] & (z > L), \end{cases} \tag{13}$$

where $\boldsymbol{r}_\perp = (x, y)$, and we have defined $\boldsymbol{k}_\perp^{(m,n)} \equiv \boldsymbol{k}_{i\perp} + \boldsymbol{G}_\perp^{(m,n)}$, with $\boldsymbol{G}_\perp^{(m,n)}$ being a 2-dimensional reciprocal vector (labeled by integers m and n and $\boldsymbol{G}_\perp^{(0,0)} = \boldsymbol{0}$) that is consistent with the

periodicity of the liquid crystal ordering, and $\boldsymbol{k}_{\mathrm{i}\perp}$ being the xy components of $\boldsymbol{k}_{\mathrm{i}}$. The wavevector component $k_{\mathrm{r},tz}^{(m,n)}$ satisfies the dispersion relation $|\boldsymbol{k}_{\perp}^{(m,n)}|^2 + (k_{\mathrm{r,\,tz}}^{(m,n)})^2 = \epsilon_{\mathrm{outside}}\,(\omega/c)^2$ $(= |\boldsymbol{k}_{\mathrm{i}}|^2)$. Here we particularly focus on normal incidence, and therefore $\boldsymbol{k}_{\mathrm{i}\perp} = 0$.

The reflectivity for each mode (m, n) is given by

$$R^{(m,n)} = -\frac{\left(\mathrm{Re}\, k_{\mathrm{rz}}^{(m,n)}\right)\left(\boldsymbol{E}_{\mathrm{r}}^{(m,n)} \cdot \boldsymbol{E}_{\mathrm{r}}^{(m,n)*}\right)}{k_{\mathrm{iz}}\left(\boldsymbol{E}_{\mathrm{i}} \cdot \boldsymbol{E}_{\mathrm{i}}^{*}\right)}, \tag{14}$$

where Re denotes the real part (for evanescent contributions, $\mathrm{Re}\, k_{\mathrm{rz}}^{(m,n)}$ and hence $R^{(m,n)}$ are zero), and the superscript * denotes the complex conjugate. Eq 14 is deduced from the z components of the Poynting vectors (Landau et al., 1984). The reflectivity to be presented below is the sum of all $R^{(m,n)}$'s in the numerical calculations.

As we are dealing with a chiral system, we are interested in the dependence of reflectivity on the sense of circular polarization of incident light. We set $\boldsymbol{E}_{\mathrm{i}} = (\sqrt{2})^{-1}(1, i, 0)$ for left-circular polarized incident light, and $\boldsymbol{E}_{\mathrm{i}} = (\sqrt{2})^{-1}(1, -i, 0)$ for right-circular polarization (We follow the convention of de Gennes and Prost 1995 for the sense of circular polarization).

Results

Structures of cholesteric blue phase in a cell

Before presenting the details of the simulation results on the structures of cholesteric blue phase cell, let us characterize the periodicity of the cholesteric blue phase structure. For this purpose, we first introduce the Fourier transform of $\chi_{\alpha\beta}(\boldsymbol{r})$:

$$\chi_{\alpha\beta}[\boldsymbol{q}] = \frac{1}{V}\int_V d\boldsymbol{r}\, \chi_{\alpha\beta}(\boldsymbol{r}) e^{i\boldsymbol{q}\boldsymbol{r}}, \tag{15}$$

whose discretized version for $\boldsymbol{q} = 2\pi(j_x/N_x\Delta_x,\, j_y/N_y\Delta_y,\, j_z/N_z\Delta_z)$ and $\boldsymbol{r} = (n_x\Delta_x,\, n_y\Delta_y,\, n_z\Delta_z)$ reads

$$\chi_{\alpha\beta}[j_x, j_y, j_z] = \frac{1}{N_x N_y N_z}\sum_{n_x=0}^{N_x-1}\sum_{n_y=0}^{N_y-1} \left\{\frac{1}{2}\left(\chi_{\alpha\beta}(n_x, n_y, 0) + \chi_{\alpha\beta}(n_x, n_y, N_z)\right) e^{2\pi i\left((j_x n_x/N_x)+\left(j_y n_y/N_y\right)\right)} + \sum_{n_z=1}^{N_z-1}\chi_{\alpha\beta}(n_x, n_y, n_z) e^{2\pi i\left((j_x n_x/N_x)+\left(j_y n_y/N_y\right)+(j_z n_z/N_z)\right)}\right\}. \tag{16}$$

Here the special treatment for $n_z = 0$ and N_z is due to the absence of periodic boundary conditions in the z direction.

Now we define the average wavenumber of the structure in the z direction by

$$\bar{q} = \frac{\overline{2\pi j_z}}{N_z\Delta_z} = \frac{\sum_{j_z}(2\pi j_z/N_z\Delta_z)\left|\chi_{\alpha\beta}[0, 0, j_z]\right|^2}{\sum_{j_z}\left|\chi_{\alpha\beta}[0, 0, j_z]\right|^2}, \tag{17}$$

and the number of periodic structures in the z (cell normal) direction:

$$m = \frac{\bar{q}L}{2\pi} = \overline{j_z}. \tag{18}$$

Note that $|\chi_{\alpha\beta}[0,\, 0,\, j_z]|^2$ is sharply peaked, and that the summation over j_z in Eq. 17 is taken over the small range containing the peak, more specifically, $40 \le j_z \le 80$, to eliminate possible undesirable contributions from higher and lower j_z (See the discussion after presenting the real-space structures in Figures 2, 3). Note also that only positive j_z is considered because $|\chi_{\alpha\beta}[0, 0, j_z]|^2 = |\chi_{\alpha\beta}[0, 0, -j_z]|^2$, and therefore the peaks appear symmetrically about $j_z = 0$).

In Figure 2 we show the representative equilibrium structures of BP I with its (110) plane parallel to the xy plane in our finite-thickness cell. It is well known that the orientational order described by a tensor order parameter is weaker at the disclination (Schopohl and Sluckin 1987), and disclination lines are depicted by the isosurfaces $\mathrm{Tr}\,\chi^2 = 0.3$ (when $\tilde{\epsilon} = 0.02$, $\mathrm{Tr}\,\chi^2 \simeq 0.69$ in the bulk away from the disclinations). Structures with different m are shown, and they are distinguished by the arrangement of disclination lines in the vicinity of the top confining surface (Figures 2A,D. See also the highlighted areas in Figures 2C,F. The bottom views, Figures 2B,E, are almost indistinguishable). The side views (Figures 2C,F) clearly indicate structures with slightly different periodicity along the z direction. The number of periodic units is in fact $m/2$, because in the definition of $\bar{q}$ (Eq. 17) spatial average in the xy directions has been taken by setting $j_x = j_y = 0$, and information on the structure in the xy directions has been lost. The lattice constant in the z direction is hence

$$a_z = \frac{2L}{m}. \tag{19}$$

Figure 3 shows two equilibrium structures of BP X with different m. The 4_1 screw axis of BP X is parallel to the z direction. Again the difference in the arrangement of disclination lines is found in the vicinity of the top surface (Figures 2A,D. Figures 2C,F also highlights the difference). Note that the disclination structure shown here has already been proposed as a candidate of BP X structure in earlier numerical studies (Alexander and Marenduzzo 2008; Alexander and Yeomans 2009).

Figure 4 shows $|\chi_{\alpha\beta}[0,\, 0,\, j_z]|^2$ for the structures shown in Figures 2, 3. Indeed, $|\chi_{\alpha\beta}[0,\, 0,\, j_z]|^2$ is sharply peaked around $m = \overline{j_z}$, and it has a smaller peak at $j_z = 0$. The latter is uninteresting for the determination of the characteristic periodicity, and therefore eliminated in the evaluation of $\overline{j_z}$ in Eq. 17 (As noted above, in the actual calculation of Eq. 17 we have

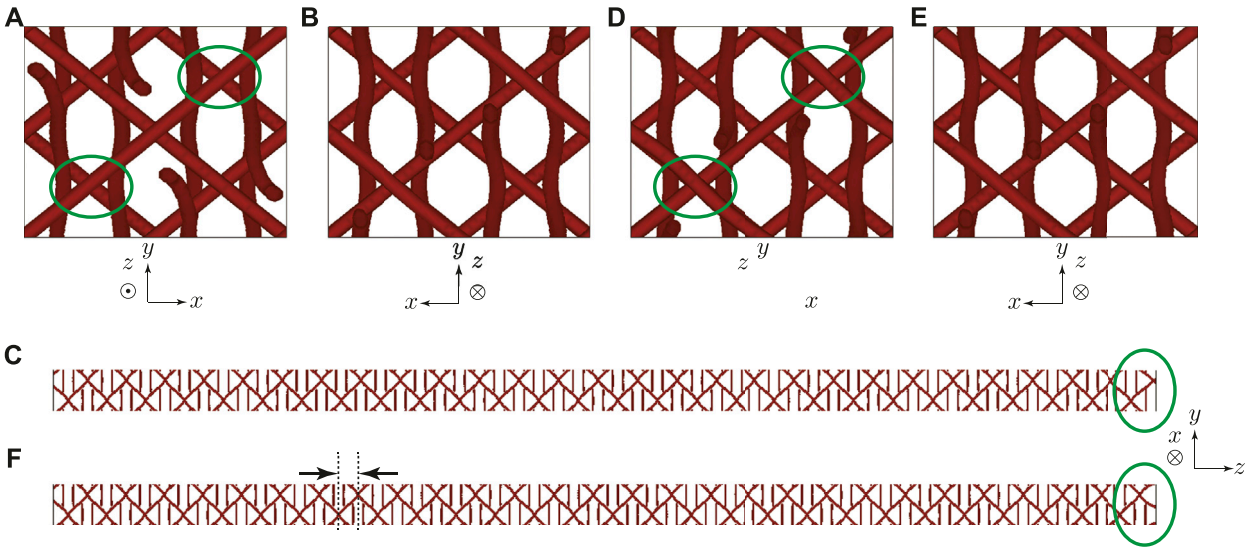

FIGURE 2
Numerically obtained BP I structures with **(A–C)** m = 56.0 and **(D–F)** m = 56.6, in orthographic view from **(A,D)** + z, **(B,E)** − z, and **(C,F)** − x direction. The interval sandwiched by arrows in **(F)** indicates the "wavelength" defined by $2\pi/\bar{q}$, which is half the lattice constant in the z direction a_z (See text). The most prominent structural differences in the top view **(A,D)** and in the sideview **(C,F)** are highlighted by ellipses. The field strength $\bar{\epsilon}$ is set to 0.02.

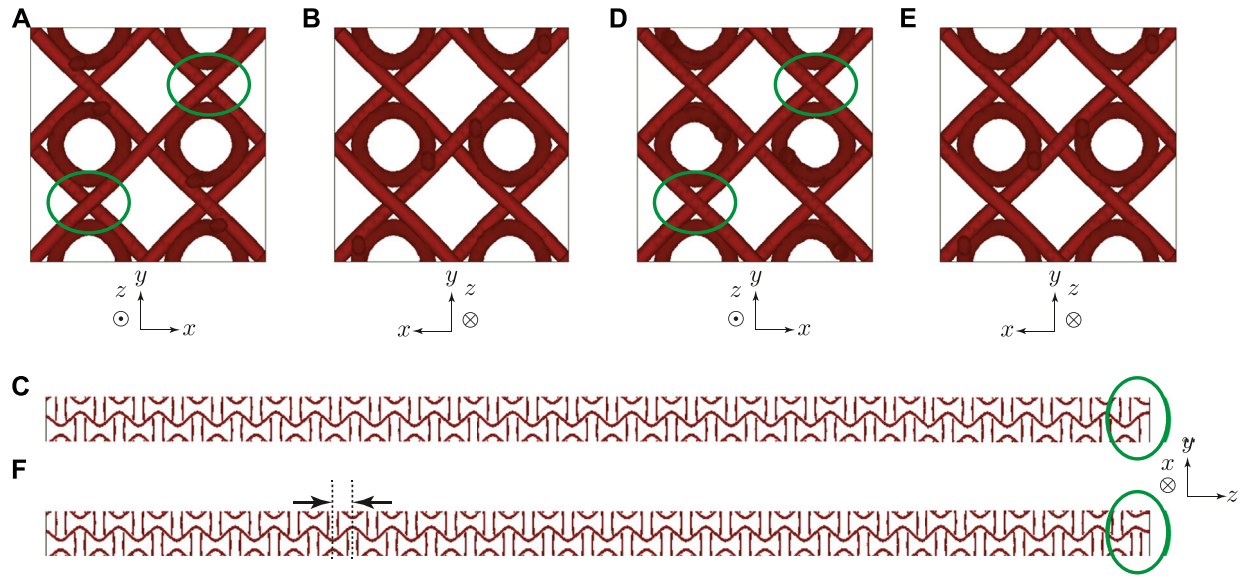

FIGURE 3
The same as Figure 2 for numerically obtained BP X structures with **(A–C)** m = 56.0 and **(D–F)** m = 56.3.

eliminated contributions from $j_z < 40$). We note that the numerator of Eq. 17 is proportional to j_z, and therefore contribution from large j_z can be non-negligible even when $|\chi_{\alpha\beta}[0, 0, j_z]|^2$ is small (We have checked that contributions from $j_z > 80$ alter $\overline{j_z}$ by 0.3–0.4). This is the reason for the elimination of contributions from $j_z > 80$ in the evaluation of Eq.

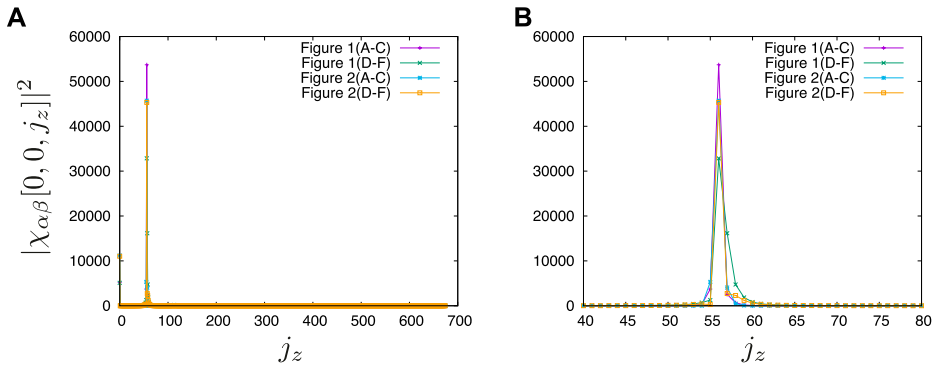

FIGURE 4
Plot of $|\chi_{\alpha\beta}[0, 0, j_z]|^2$ as a function of j_z for the structures in Figures 2, 3. The range of j_z is **(A)** $j_z \geq 0$ and **(B)** $40 \leq j_z \leq 80$.

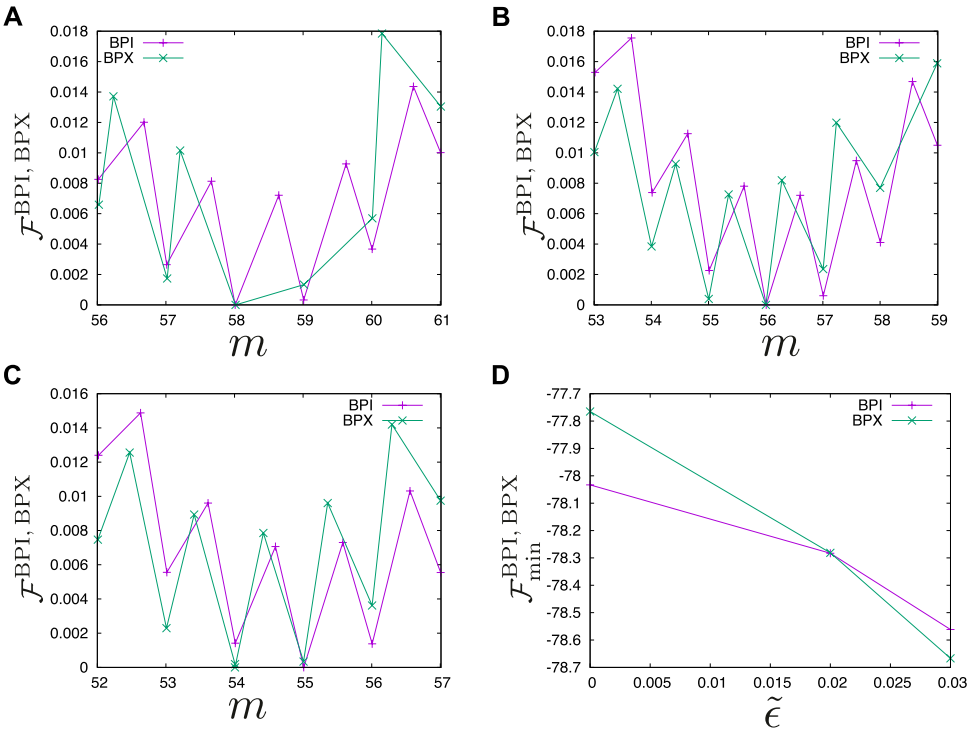

FIGURE 5
The free energy of the BP cell $\mathcal{F}^{\mathrm{BPI,BPX}}(m,\tilde{\epsilon}) - \mathcal{F}^{\mathrm{BPI,BPX}}_{\mathrm{min}}(\tilde{\epsilon})$ as a function of m, for $\tilde{\epsilon}$ = **(A)** 0, **(B)** 0.02 and **(C)** 0.03. **(D)** Plot of $\mathcal{F}^{\mathrm{BPI,BPX}}_{\mathrm{min}}$ as a function of $\tilde{\epsilon}$.

17. As we will see in Figure 5, $\overline{j_z}\,(=m)$ falls within the range $40 \leq \overline{j_z} \leq 80$, and therefore the above-mentioned elimination does not miss the contribution from the sharp peak of interest.

To show how the free energy of the BP cell per unit area (hereafter denoted by $\mathcal{F}^{\mathrm{BPI}}$ and $\mathcal{F}^{\mathrm{BPX}}$ for BP I and BP X structures, respectively, and calculated by Eq. 9) depends on m that characterizes the periodicity of the BP structure, we plot in Figure 5A–C the dependence of $\mathcal{F}^{\mathrm{BPI}}$ and $\mathcal{F}^{\mathrm{BPX}}$ on m for different field strengths $\tilde{\epsilon}$. In Figure 5A–C, the free energy is subtracted by the minimum free energy for given structure and $\tilde{\epsilon}$, which is denoted by $\mathcal{F}^{\mathrm{BPI,BPX}}_{\mathrm{min}}(\tilde{\epsilon})$. In Figure 5D, we separately show $\mathcal{F}^{\mathrm{BPI,BPX}}_{\mathrm{min}}(\tilde{\epsilon})$.

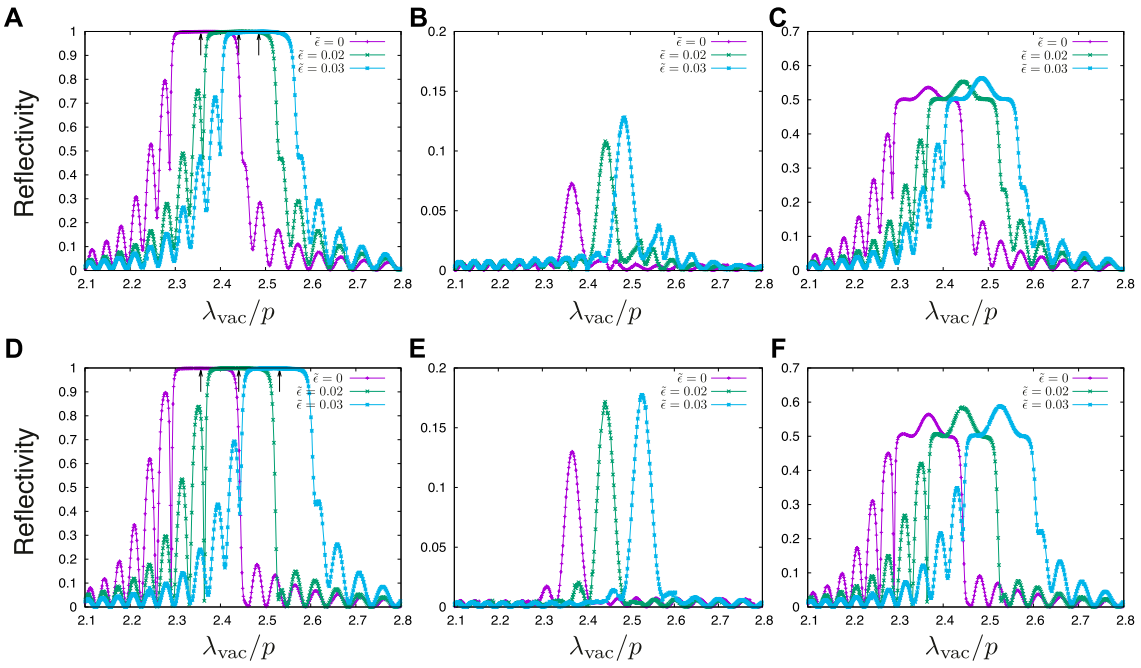

FIGURE 6
Reflection spectra for **(A–C)** BP I structures for $\tilde{\epsilon} = 0$ ($m = 58$), $\tilde{\epsilon} = 0.02$ ($m = 56$) and $\tilde{\epsilon} = 0.03$ ($m = 55$), and **(D–F)** BP X structures for $\tilde{\epsilon} = 0$ ($m = 58$), $\tilde{\epsilon} = 0.02$ ($m = 56$) and $\tilde{\epsilon} = 0.03$ ($m = 54$). The polarization of the normally incident light is **(A,D)** right-circular (the same as the sense of the twisted orientational ordering), **(B,E)** left-circular, and **(C,F)** unpolarized. The horizontal axis is the wavelength of incident light in vacuum, λ_{vac}, divided by the cholesteric pitch p. Arrows in **(A,D)** indicates λ_{vac}/p with $\lambda_{vac} = a_z{}^* n_{LC}$ and $n_{LC} = 1.6$.

One finds that the local minima of $\mathcal{F}^{BPI}$ and $\mathcal{F}^{BPX}$ are found at integer m's (To be precise, "m is an integer" means that the difference between m and the closest integer is smaller than 0.025).Figure 2A–C. Figure 3A–C show typical structures with integer m. For non-integer m's $\mathcal{F}^{BPI}$ and $\mathcal{F}^{BPX}$ exhibit local maximum, and the corresponding structures inFigure 2D–F. Figure 3D–F. The relaxation of initial structures described in *Calculation of BP structures* results in these types of structures, and hence m cannot take continuous values, but is discretized, as can be clearly seen in Figures 5A–C. Note that in our calculations metastable profiles for BP X could not be reached in the intervals $58 < m < 59$ and $59 < m < 60$ in Figure 5A, and $58 < m < 59$ in Figure 5B; the initial profiles prepared for the intervals turned out to relax to structures with integer m. Since in an infinite system without boundaries the lattice constant along the field direction a_z is expected to take only one optimum value for a given BP structure and a field strength, the observation that the BP can take multiple discrete values of m (and hence a_z) is clearly attributable to the presence of confining surfaces. Such discretization of BP structures was reported in our previous numerical study for different anchoring condition and smaller cell thickness (Fukuda and Žumer 2011c).

From Figure 5 we also find that stronger $\tilde{\epsilon}$ (or the electric field) drives the optimum m to smaller values (i.e., larger a_z), indicating electrostriction, and that the optimum m is common for BP I and BP X (58 for $\tilde{\epsilon} = 0$ and 56 for $\tilde{\epsilon} = 0.02$) except for $\tilde{\epsilon} = 0.03$ (55 for BP I and 54 for BP X). Note that $\mathcal{F}(m, \tilde{\epsilon}) - \mathcal{F}_{min}(\tilde{\epsilon})$ for BP X is smaller than that for BP I when m is smaller than the optimum value, which indicates that BP X is inclined to exhibit structures with larger a_z.

Figure 5D demonstrates that a stronger field favors BP X, and the transition between BP I and BP X is located at $\tilde{\epsilon} \simeq 0.02$, close to that in the bulk (As noted in *Calculation of BP structures*, $\tilde{\epsilon} = 0.02$ corresponds to $E \simeq 3.2$ V/μm, and the experimental BP I–BP X transition in Guo et al., 2020 is at $\simeq 3.0$ V/μm).

Guo et al., 2020 showed that BP X structures carefully prepared by applying an electric field can retain their ordering even after the cessation of the field, despite the energy gain by the transformation to BP I (estimated to be $\simeq 1.8 \times 10^4 k_B T/\mu m^2$ from Figure 5D; Eq. 10). We first note that from our numerical results we cannot evaluate the energy barrier involved in the structural transformation from BP X to BP I, because its kinetic pathway is not clear. Nevertheless we comment that in the relaxation process to obtain the (meta)stable profiles we did not observe

spontaneous transformation from BP X to BP I, suggesting non-negligible energy barriers. Now let us discuss the energy barrier involved in the variation of m or a_z. Suppose that the BP X structure with $m = 56$ is transformed to BP I with the same m after the electric field with $\tilde{\epsilon} = 0.02$ is turned off. From Figure 5A; Eq. 10, the energy barrier experienced by the transformation of BP I from $m = 56$ to 57 is $\Delta\mathcal{F} \simeq 3.8 \times 10^{-3}$, corresponding to $\simeq 260 k_B T/\mu\text{m}^2$. When the BP X structure is retained, this energy barrier is still larger ($\Delta\mathcal{F} \simeq 7.1 \times 10^{-3}$ corresponding to $\simeq 480 k_B T/\mu\text{m}^2$). We are dealing with a perfect lattice realized by periodic boundaries in the xy directions, and in actual experiments lattice imperfections would lower the energy barrier towards the original a_z (This could be why metastable BPs with different lattice constant had not been observed before Guo et al., 2020). On the contrary, our results indicate that a perfect BP ordering with a_z (or m) being not optimized can be stable enough over thermal fluctuations.

Reflection spectra

Here we consider how the BP cell reflects normally incident light, and Figure 6 shows the reflection spectra for the BP I and BP X structures that minimize the free energy and are presented in *Structures of cholesteric blue phase in a cell*. The horizontal axis represents λ_{vac}/p, where λ_{vac} is the wavelength of the incident light in vacuum, given by $2\pi n_{\text{outside}}/|\boldsymbol{k}_i|$. Irrespective of whether the structure is BP I or BP X, when the sense of the polarization is the same as that of the twisted orientational order (right-circular in the present study), strong selective reflection occurs (Figures 6A,D) and otherwise reflection becomes much weaker (Figures 6B,E). Strong selective reflection of circularly polarized light has long been well known for a cholesteric liquid crystal cell (Berreman and Scheffer 1970; Dreher et al., 1971; Takezoe et al., 1983; de Gennes and Prost 1995; St. John et al., 1995), and similar selective reflection by BPs has been also drawing interest (Bohley and Scharf 2004; Yoshida et al., 2016; Cho et al., 2021). Reflection spectra for unpolarized light are also shown in Figures 6C,F that could be compared with some experiments.

When the electric field is stronger, and the lattice spacing in the z direction, a_z, becomes larger, the shift of the reflection peak towards larger λ_{vac} is clearly observed, as expected and in agreement with experiments (Heppke et al., 1989b; Yoshida et al., 2013; Chen et al., 2015; Guo et al., 2020). The location of the peak agrees with that of the Bragg peak $\lambda_{\text{vac}} = a_z n_{\text{LC}}$ (See the arrows in Figures 6A,D). When the BP X structure with $m = 56$ turns out to be stable, the peak shift from that of BP I with no field ($m = 58$) is $\simeq 3.6\%$, close to the typical values reported in Guo et al., 2020, again suggesting that the discretization of the BP structure by the confining surfaces is responsible for the stabilization of the BP structure with different lattice constant in Guo et al., 2020.

We note that the qualitative difference in shape between the reflection spectra of BP I (Figures 6A–C)) and BP X (Figures 6D–F)) is not pronounced. Therefore reflection spectra for normal incident alone cannot distinguish the structural difference of BPs, and other techniques such as Kossel diagrams (Heppke et al., 1989b; Yoshida et al., 2013; Chen et al., 2015; Guo et al., 2020) will be necessary. We further note that, in contrast to our calculation results (Figure 6), in many experiments the reflection spectra are bell-shaped, and that the fringes are not observed or far less visible if they exist. This difference could be due to the perfect ordering in our calculation not realized in experiments, a small distribution of the incident angle in experiments, or the fluctuation of the cholesteric pitch (St. John et al., 1995).

Discussion

We carried out a simulation study on the structures and optical properties of a cholesteric blue phase cell whose thickness is on the order of 10 μm, comparable to that of typical experimental systems, and much larger than that of previous simulation studies. Our numerical calculations were based on the Landau-de Gennes continuum theory describing the orientational order by a second-rank tensor. We focused on two blue phase structures: One is BP I with its (110) plane parallel to the confining surfaces, and the other is BP X with its 4_1 screw axis along the cell normal. The latter has been known to be not thermodynamically stable in the absence of an electric field. We were particularly interested in the effect of the applied electric field along the cell normal.

We showed that both BP I and BP X exhibit multiple (meta) stable structures with a different value of the lattice constant in the cell normal direction. The possibility of multiple states with distinct lattice constant is attributable to the presence of confining planes. The electrostriction, larger lattice constant along the field direction for a stronger field, was also clearly observed. From the evaluation of the free energy, we found that the (meta)stable structures of BP I and BP X can be stable enough with respect to the variation of the lattice constant in the cell normal. We also calculated the reflection spectra of these blue phase structures for normal incident light, and demonstrated the selective reflection of circularly polarized light arising from the chirality of the blue phase structure, and the shift of reflection peak due to electrostriction. These findings are in qualitative agreement with recent experimental results reported in Guo et al., 2020 on the stabilization of BP X structures with different reflection peak wavelength. The relative shift of the peak wavelength of a few percent in Guo et al., 2020 is safely accounted for by the discretization of the BP structure we found numerically.

Here we particularly focused on BP I, and the other cubic structure BP II is also expected to exhibit discretized behavior attributable to the cell surfaces, although further experimental and numerical studies will be necessary. How the presence of cell surfaces affects BP III that is believed to be amorphous is far from trivial, and because one cannot assume periodicity in the lateral directions, numerical calculations for BP III will be much more challenging, and experimental studies are first desirable.

As mentioned above, our study concerns only cases with specific orientation of the BP lattice, and there are other possibilities of lattice orientations (Kitzerow 1991; Miller and Gleeson 1996). Which lattice orientation is more easily realized in a BP cell of finite thickness, and how the lattice orientation with respect to the confining surfaces affects the response of BPs to an electric field will be interesting future directions of numerical studies.

We restricted ourselves to the (meta)stable static structures, and the investigation of dynamic behavior in a realistic time scale is a daunting task requiring an unrealistically long calculation time: In Guo et al., 2020 the duration of the electric field is tens of seconds, and in our present numerical system, simulation of the dynamics for 1 s will take almost 2 years (in some of the calculations we used 56 cores of Intel Xeon Gold 6330 CPU with OpenMP parallelization). We note that the incorporation of the backflow, not taken into account in our dynamic Equation (11), will further slow the calculation. Moreover, Guo et al., 2020 emphasized the importance of the application of the field without heating the liquid crystal. Most of the simulations based on the Landau-de Gennes formalism (including ours) assume an isothermal system, and incorporation of the effect of heating requires the formulation of the dynamics of the liquid crystal including inhomogeneous temperature field. Although such formalism based on non-equilibrium thermodynamics has been developed for a long time (Martin et al., 1972; De Groot and Mazur 1984), simulating liquid crystals with spatial variation of temperature does not seem to be drawing particular attention.

As mentioned above, simulation of the dynamics of a blue phase cell of realistic size and time scale is highly challenging. Nevertheless, our study reveals the necessity of such studies for the understanding of the behavior of a blue phase cell, especially when one is interested in its practical application.

Data availability statement

The raw data supporting the conclusion of this article will be made available by the authors, without undue reservation.

Author contributions

J-iF designed and carried out the study, and wrote the manuscript.

Funding

This work is supported by JSPS KAKENHI (Grant Numbers JP17H02947 and JP21H01049), and JSPS Bilateral Joint Research Project between Japan and Slovenia led by Professor Tomonari Dotera and Professor Primož Ziherl.

Acknowledgments

The author thanks Professor Slobodan Žumer for valuable discussions and suggestions that motivated the present study. Part of the numerical calculations was carried out using the facilities of the Supercomputer Center, the Institute for Solid State Physics, the University of Tokyo.

Conflict of interest

The author declares that the research was conducted in the absence of any commercial or financial relationships that could be construed as a potential conflict of interest.

Publisher's note

Supplementary material

The Supplementary Material for this article can be found online at: https://www.frontiersin.org/articles/10.3389/frsfm.2022.1011618/full#supplementary-material

References

Alexander, G. P., and Marenduzzo, D. (2008). Cubic blue phases in electric fields. *Europhys. Lett.* 81, 66004. doi:10.1209/0295-5075/81/66004

Alexander, G. P., and Yeomans, J. M. (2009). Numerical results for the blue phases. *Liq. Cryst.* 36, 1215–1227. doi:10.1080/02678290903057390

Bahr, C., and Kitzerow, H.-S. (2001). *Chirality in liquid crystals*. Springer.

Berreman, D. W., and Scheffer, T. J. (1970). Bragg reflection of light from single-domain cholesteric liquid-crystal films. *Phys. Rev. Lett.* 25, 577–581. doi:10.1103/PhysRevLett.25.577

Bohley, C., and Scharf, T. (2004). Polarization of light reflected by cholesteric blue phases. *J. Opt. A Pure Appl. Opt.* 6, S77–S80. doi:10.1088/1464-4258/6/3/014

Chen, C.-W., Li, C.-C., Jau, H.-C., Yu, L.-C., Hong, C.-L., Guo, D.-Y., et al. (2015). Electric field-driven shifting and expansion of photonic band gaps in 3D liquid photonic crystals. *ACS Photonics* 2, 1524–1531. doi:10.1021/acsphotonics.5b00314

Cho, S., Takahashi, M., Fukuda, J., Yoshida, H., and Ozaki, M. (2021). Directed self-assembly of soft 3d photonic crystals for holograms with omnidirectional circular-polarization selectivity. *Commun. Mat.* 2, 39. doi:10.1038/s43246-021-00146-x

Cladis, P. E., Garel, T., and Pieranski, P. (1986). Kossel diagrams show electric-field-induced cubic-tetragonal structural transition in frustrated liquid-crystal blue phases. *Phys. Rev. Lett.* 57, 2841–2844. doi:10.1103/PhysRevLett.57.2841

de Gennes, P. G., and Prost, J. (1995). "The Physics of liquid crystals," in *International series of monographs on Physics*. 2 edn (Oxford: Oxford University).

De Groot, S., and Mazur, P. (1984). *Non-equilibrium thermodynamics*. Dover Books on Physics Dover Publications.

Dreher, R., Meier, G., and Saupe, A. (1971). Selective reflection by cholesteric liquid crystals. *Mol. Cryst. Liq. Cryst.* 13, 17–26. doi:10.1080/15421407108083534

Fournier, J.-B., and Galatola, P. (2005). Modeling planar degenerate wetting and anchoring in nematic liquid crystals. *Europhys. Lett.* 72, 403–409. doi:10.1209/epl/i2005-10253-5

Fukuda, J. (2022). Exotic structures of a thin film of chiral liquid crystals: A numerical study based on the Landau–de Gennes theory. *Liq. Cryst. Rev.*. doi:10.1080/21680396.2022.2077256

Fukuda, J., Nych, A., Ognysta, U., Žumer, S., and Muševič, I. (2022). Liquid crystalline half-skyrmions and their optical properties. *Ann. Phys.* 534, 2100336. doi:10.1002/andp.202100336

Fukuda, J., Nych, A., Ognysta, U., Žumer, S., and Muševič, I. (2018). Liquid-crystalline half-skyrmion lattice spotted by kossel diagrams. *Sci. Rep.* 8, 17234. doi:10.1038/s41598-018-35514-0

Fukuda, J., Okumura, Y., and Kikuchi, H. (2016). Calculation of confocal microscope images of cholesteric blue phases. *Proc. SPIE* 9769, 976906. doi:10.1117/12.2209210

Fukuda, J., Yoneya, M., and Yokoyama, H. (2009). Simulation of cholesteric blue phases using a Landau–de Gennes theory: Effect of an applied electric field. *Phys. Rev. E* 80, 031706. doi:10.1103/PhysRevE.80.031706

Fukuda, J., and Žumer, S. (2010a). Cholesteric blue phases: Effect of strong confinement. *Liq. Cryst.* 37, 875–882. doi:10.1080/02678292.2010.481909

Fukuda, J., and Žumer, S. (2010b). Novel defect structures in a strongly confined liquid-crystalline blue phase. *Phys. Rev. Lett.* 104, 017801. doi:10.1103/PhysRevLett.104.017801

Fukuda, J., and Žumer, S. (2011a). Quasi-two-dimensional Skyrmion lattices in a chiral nematic liquid crystal. *Nat. Commun.* 2, 246. doi:10.1038/ncomms1250

Fukuda, J., and Žumer, S. (2011b). Ring defects in a strongly confined chiral liquid crystal. *Phys. Rev. Lett.* 106, 097801. doi:10.1103/PhysRevLett.106.097801

Fukuda, J., and Žumer, S. (2011c). Structural forces in liquid crystalline blue phases. *Phys. Rev. E* 84, 040701. doi:10.1103/PhysRevE.84.040701

Fukuda, J., and Žumer, S. (2013). Field-induced dynamics and structures in a cholesteric-blue-phase cell. *Phys. Rev. E* 87, 042506. doi:10.1103/PhysRevE.87.042506

Fukuda, J., and Žumer, S. (2018). Reflection spectra and near-field images of a liquid crystalline half-skyrmion lattice. *Opt. Express* 26, 1174–1184. doi:10.1364/OE.26.001174

Fukuda, J., and Žumer, S. (2020). Lattice orientation of cholesteric blue phases in contact with surfaces enforcing unidirectional planar anchoring. *Phys. Rev. Res.* 2, 033407. doi:10.1103/PhysRevResearch.2.033407

Gandhi, S. S., and Chien, L.-C. (2017). Unraveling the mystery of the blue fog: Structure, properties, and applications of amorphous blue phase iii. *Adv. Mat.* 29, 1704296. doi:10.1002/adma.201704296

Guo, D.-Y., Chen, C.-W., Li, C.-C., Jau, H.-C., Lin, K.-H., Feng, T.-M., et al. (2020). Reconfiguration of three-dimensional liquid-crystalline photonic crystals by electrostriction. *Nat. Mat.* 19, 94–101. doi:10.1038/s41563-019-0512-3

Henrich, O., Marenduzzo, D., Stratford, K., and Cates, M. E. (2010). Thermodynamics of blue phases in electric fields. *Phys. Rev. E* 81, 031706. doi:10.1103/PhysRevE.81.031706

Henrich, O., Stratford, K., Cates, M. E., and Marenduzzo, D. (2011). Structure of blue phase III of cholesteric liquid crystals. *Phys. Rev. Lett.* 106, 107801. doi:10.1103/PhysRevLett.106.107801

Heppke, G., Jérôme, B., Kitzerow, H.-S., and Pieranski, P. (1989a). Electrostriction of bpi and bpii for blue phase systems with negative dielectric anisotropy. *J. Phys. Fr.* 50, 549–562. doi:10.1051/jphys:01989005005054900

Heppke, G., Jérôme, B., Kitzerow, H.-S., and Pieranski, P. (1989b). Electrostriction of the cholesteric blue phases bpi and bpii in mixtures with positive dielectric anisotropy. *J. Phys. Fr.* 50, 2991–2998. doi:10.1051/jphys:0198900500190299100

Hornreich, R. M., and Shtrikman, S. (1989). Invited Lecture. Hexagonal cholesteric blue phases. *Liq. Cryst.* 5, 777–789. doi:10.1080/02678298908026384

Kikuchi, H., Higuchi, H., Haseba, Y., and Iwata, T. (2007). 62.2: Invited paper: Fast electro-optical switching in polymer-stabilized liquid crystalline blue phases for display application. *SID Symposium Dig. Tech. Pap.* 38, 1737–1740. doi:10.1889/1.2785662

Kikuchi, H., Yokota, M., Hisakado, Y., Yang, H., and Kajiyama, T. (2002). Polymer-stabilized liquid crystal blue phases. *Nat. Mat.* 1, 64–68. doi:10.1038/nmat712

Kitzerow, H.-S. (1991). The effect of electric fields on blue phases. *Mol. Cryst. Liq. Cryst.* 202, 51–83. doi:10.1080/00268949108035659

Landau, L. D., Lifshitz, E., and Pitaevskii, L. (1984). *Electrodynamics of continuous media*. 2 edn, 8. Elsevier.

Li, X., Martínez-González, J. A., Hernández-Ortiz, J. P., Ramírez-Hernández, A., Zhou, Y., Sadati, M., et al. (2017). Mesoscale martensitic transformation in single crystals of topological defects. *Proc. Natl. Acad. Sci. U. S. A.* 114, 10011–10016. doi:10.1073/pnas.1711207114

Martin, P. C., Parodi, O., and Pershan, P. S. (1972). Unified hydrodynamic theory for crystals, liquid crystals, and normal fluids. *Phys. Rev. A* 6, 2401–2420. doi:10.1103/PhysRevA.6.2401

Martínez-González, J. A., Li, X., Sadati, M., Zhou, Y., Zhang, R., Nealey, P. F., et al. (2017). Directed self-assembly of liquid crystalline blue-phases into ideal single-crystals. *Nat. Commun.* 8, 15854. doi:10.1038/ncomms15854

Miller, R. J., and Gleeson, H. F. (1996). Lattice parameter measurements from the Kossel diagrams of the cubic liquid crystal blue phases. *J. Phys. II Fr.* 6, 909–922. doi:10.1051/jp2:1996219

Nych, A., Fukuda, J., Ognysta, U., Žumer, S., and Muševič, I. (2017). Spontaneous formation and dynamics of half-skyrmions in a chiral liquid-crystal film. *Nat. Phys.* 13, 1215–1220. doi:10.1038/nphys4245

Pieranski, P., Cladis, P., and Barbet-Massin, R. (1985). Experimental evidence for a hexagonal blue phase. *J. Phyique. Lett.* 46, 973–977. doi:10.1051/jphyslet:019850046020097300

Pieranski, P., and Cladis, P. E. (1987). Field-induced tetragonal blue phase (BP X). *Phys. Rev. A* 35, 355–364. doi:10.1103/PhysRevA.35.355

Rahman, M. D. A., Said, S. M., and Balamurugan, S. (2015). Blue phase liquid crystal: Strategies for phase stabilization and device development. *Sci. Technol. Adv. Mater.* 16, 033501. doi:10.1088/1468-6996/16/3/033501

Schopohl, N., and Sluckin, T. J. (1987). Defect core structure in nematic liquid crystals. *Phys. Rev. Lett.* 59, 2582–2584. doi:10.1103/PhysRevLett.59.2582

St. John, W. D., Fritz, W. J., Lu, Z. J., and Yang, D.-K. (1995). Bragg reflection from cholesteric liquid crystals. *Phys. Rev. E* 51, 1191–1198. doi:10.1103/PhysRevE.51.1191

Takezoe, H., Ouchi, Y., Hara, M., Fukuda, A., and Kuze, E. (1983). Experimental studies on reflection spectra in monodomain cholesteric liquid crystal cells: Total reflection, subsidiary oscillation and its beat or swell structure. *Jpn. J. Appl. Phys. (2008).* 22, 1080–1091. doi:10.1143/jjap.22.1080

Tan, G., Lee, Y.-H., Gou, F., Chen, H., Huang, Y., Lan, Y.-F., et al. (2017). Review on polymer-stabilized short-pitch cholesteric liquid crystal displays. *J. Phys. D. Appl. Phys.* 50, 493001. doi:10.1088/1361-6463/aa916a

Tiribocchi, A., Gonnella, G., Marenduzzo, D., and Orlandini, E. (2011a). Switching dynamics in cholesteric blue phases. *Soft Matter* 7, 3295–3306. doi:10.1039/C0SM00979B

Tiribocchi, A., Gonnella, G., Marenduzzo, D., Orlandini, E., and Salvadore, F. (2011b). Bistable defect structures in blue phase devices. *Phys. Rev. Lett.* 107, 237803. doi:10.1103/PhysRevLett.107.237803

Wright, D. C., and Mermin, N. D. (1989). Crystalline liquids: The blue phases. *Rev. Mod. Phys.* 61, 385–432. doi:10.1103/RevModPhys.61.385

Yoshida, H., Anucha, K., Ogawa, Y., Kawata, Y., Ozaki, M., Fukuda, J., et al. (2016). Bragg reflection band width and optical rotatory dispersion of cubic blue-phase liquid crystals. *Phys. Rev. E* 94, 042703. doi:10.1103/PhysRevE.94.042703

Yoshida, H., Yabu, S., Tone, H., Kikuchi, H., and Ozaki, M. (2013). Electro-optics of cubic and tetragonal blue phase liquid crystals investigated by two-beam interference microscopy. *Appl. Phys. Express* 6, 062603. doi:10.7567/apex.6.062603